Journal of Materials Chemistry A

ROYAL SOCIETY OF CHEMISTRY

PAPER

View Article Online
View Journal

Check for updates

Cite this: DOI: 10.1039/d5ta04447b

Plasma-derived hydrogen radical-mediated N_2 activation for mild ammonia synthesis: insights into the importance of oxygen vacancies in the reaction mechanism

Shijian Luo, †[a] Yongduo Liu,†[a] Lin Guo,†[b] Yang Song, [a] Yuran Yang,[a] Fadong Chen,[a] Linhu Wang,[c] Yanan Chen,*[cde] Siguo Chen *[a] and Zidong Wei [a]

Plasma-catalytic NH_3 synthesis has recently been recognized as a complementary route to the Haber–Bosch process for decentralized NH_3 production. However, the activation of N_2 in current plasma catalysis studies is still occurs through the conventional heterogeneous reaction mechanism on catalyst surfaces, which does not take full advantage of the highly reactive species generated in the plasma phase, resulting in high energy consumption and low reaction rate. Here, we present a distinctive hydrogen radical-mediated N_2 activation pathway that extricates itself from the conventional catalytic pathways. In this work, a considerable number of gaseous hydrogen radicals were generated on an oxygen-deficient CeO_2/CuO catalyst *via* the excitation of plasma and served as strong reducing agents and immediate hydrogen sources to reduce N_2 molecules with an ultralow energy barrier of 0.123 eV. Oxygen vacancies on catalysts can further accelerate the catalytic cycling of adsorbed H_2 to desorbed hydrogen radicals. With these strategies, we achieved a superhigh NH_3 yield of 196.2 mg h^{-1} $g_{cat.}^{-1}$ under mild conditions. Our results illustrate the potential of exploiting plasma-derived hydrogen radicals as ideal and homogeneous activation agents for inert gas molecules and introduce a design strategy for catalysts that utilize oxygen vacancies to assist hydrogen radical generation.

Received 3rd June 2025
Accepted 4th August 2025

DOI: 10.1039/d5ta04447b

rsc.li/materials-a

Published on 05 August 2025. Downloaded by Yunnan University on 8/23/2025 4:21:29 PM.

Introduction

Ammonia (NH_3) is a pivotal component in fertilizers and fine chemicals and is currently seen as an ideal carbon-free fuel and clean energy carrier.[1] To date, the Haber–Bosch method is the dominant method used for the industrial production of NH_3.[2] Although this process can reach a superhigh NH_3 synthesis rate of 10^5 mg h^{-1} g^{-1}, it needs to meet the harsh reaction conditions of high temperature and high pressure and remains heavily dependent on fossil fuels, resulting in significant CO_2 emissions.[3,4] To develop a greener synthetic route, tremendous effort has been made to explore other approaches, such as electrocatalysis,[5] photocatalysis,[6] and plasma catalysis.[7,8] These alternatives directly using nitrogen (N_2) and hydrogen (H_2) from renewable sources provide a simple and clean approach that can be based on renewably generated electricity, which will enable eco-friendly and decentralized NH_3 production as well as compatibility with intermittent renewable energy. Furthermore, the ammonia yield of these new methods (approximately 10^1–10^2 mg h^{-1} g^{-1}) is comparable to that of the Haber–Bosch process under the mild reaction conditions of low temperature and atmospheric pressure.[9,10] Therefore, these new methods are regarded as important complementary technologies to industrial NH_3 production. Unfortunately, in most of the reported studies, the dissociation and hydrogenation of N_2 are always restricted to the heterogeneous catalyst surface.[11–14] The adsorbed N_2 molecules must overcome a high energy barrier to be dissociated and hydrogenated to form crucial surface intermediates with high adsorption strength under even the activation effect of the catalyst.[15] Worse yet, the low temperature and atmospheric pressure conditions used in the new approaches, especially the electrocatalysis and photocatalysis approaches with electrolytes with ultralow N_2 solubility, hardly supply a sufficient concentration of inert N_2 gas to be adsorbed onto

[a]State Key Laboratory of Advanced Chemical Power Sources (SKL-ACPS), School of Chemistry and Chemical Engineering, Center of Advanced Electrochemical Energy (CAEE), Institute of Advanced Interdisciplinary Studies, Chongqing University, Chongqing, 401331, China. E-mail: csg810519@126.com

[b]SINOPEC Research Institute of Petroleum Processing Co., Ltd, Beijing, 100083, China

[c]Ningbo Yonglin Electron Electrical Equipment Co., Ltd, Hengxi Industrial Zone, Yinzhou District, Ningbo City, Zhejiang, 315131, China. E-mail: chenyanan@wtbu.edu.cn

[d]Institute of Renewable Energy and Energy Storage Technology, Wuhan Technology and Business University, No. 3 Huangjiahu West Road, Hongshan District, Wuhan, 430065, China

[e]Chongqing Key Laboratory of Chemical Process for Clean Energy and Resource Utilization, School of Chemistry and Engineering, Chongqing University, Shazhengjie 174, Chongqing, 400044, China

† These authors contributed equally to this work.

Published on 05 August 2025. Downloaded by Yunnan University on 8/23/2025 4:21:29 PM.

the catalyst surface. The insufficient supply of reactants, the limited adsorption sites on the catalyst surface, the competitive adsorption of intermediates, and the high energy barriers of N_2 dissociation/hydrogenation have profoundly limited the rate and efficiency of N_2 activation,[16,17] and ultimately resulted in a low NH_3 synthesis rate. It is apparent from current synthesis methods that achieving efficient NH_3 synthesis under mild reaction conditions is still very challenging.

Unlike conventional thermochemical catalysis, plasma catalysis is expected to offer unique molecular activation modes and reaction mechanisms, circumventing the complex and slow heterogeneous reaction mechanism on catalyst surfaces.[18] In plasma catalysis, high-energy electrons collide with reactant molecules in the gas phase and/or on the catalyst surface, generating numerous chemically reactive species (free radicals, ions, excited atoms or molecules). This process offers a unique advantage by enabling reactions that are typically difficult to occur under thermal equilibrium conditions, while significantly accelerating them under relatively mild conditions.[19] However, in most studies, these reactive species subsequently adsorb onto the catalyst surface and combine *via* the conventional Eley–Rideal (E–R) and Langmuir–Hinshelwood (L–H) mechanisms.[19] Accordingly, the design principles of current catalysts adhere to the conventional catalyst guidelines, which do not take into account the fact that plasma-derived reactive species may directly participate as reactants in NH_3 synthesis within the gas-plasma phase, thereby allowing catalytic reactions to proceed through entirely different reaction pathways. Therefore, it is crucial to develop a new strategy that maximizes the advantages of plasma catalysis in generating highly reactive species and improves the efficiency of NH_3 synthesis. Based on this analysis, we propose to establish an ideal catalytic system, which enhances the generation of highly reactive species through the synergistic effect between catalysts and plasma, thereby ultimately circumventing the complex and slow heterogeneous reaction pathway on catalyst surfaces.

Herein, we report an unprecedented N_2 activation pathway that extricates itself from the conventional heterogeneous catalytic pathways restricted to the catalyst surface. In this work, a considerable number of gaseous hydrogen radicals were generated on oxygen-deficient CeO_2/CuO catalysts *via* the excitation of plasma and served as strong reducing agents and immediate hydrogen sources to reduce N_2 molecules with an ultralow energy barrier of 0.123 eV (Fig. 1). Oxygen vacancies can accelerate the catalytic cycling of adsorbed H_2 to desorbed hydrogen radicals, which is essential for promoting the hydrogenation reduction process of N_2 molecules. This strategy not only enables N_2 molecules being activated throughout the entire gas–plasma phase space, but also shifts the rate-determining step (RDS) from the high-energy-barrier N_2 dissociation to the generation of hydrogen radicals, which is associated with a low formation energy. Benefiting from the above advantages, a superhigh NH_3 yield of 196.2 mg h^{-1} $g_{cat.}{}^{-1}$ was achieved by the collective effect of catalyst and plasma, exhibiting preliminary potential for industrial applications.

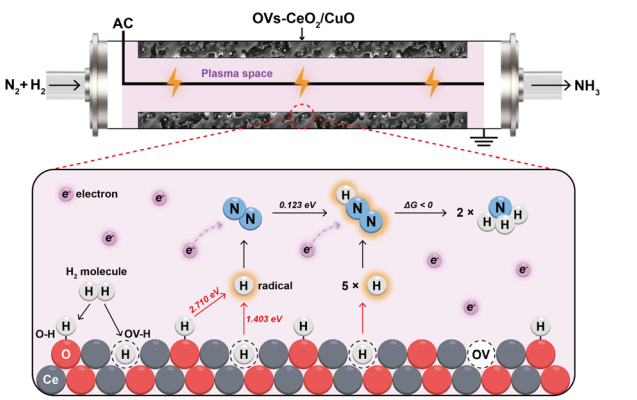

Fig. 1 Schemes of plasma-derived hydrogen radical-mediated N_2 activation for ammonia synthesis.

Results and discussion

Density functional theory (DFT) calculations were first carried out to screen for the optimal thermodynamic N_2 activation pathway by calculating the formation energies of highly reactive H and N species under plasma conditions.[20] As shown in Fig. 2a, b and Table S1, the dissociation pathway leading to the formation of H radicals from H_2 exhibits the lowest energy barrier of 3.996 eV. This value is significantly lower than those required for H_2 ionization (15.426 eV),[21] H_2 dissociative ionization (17.595 eV for $H + H^+$, 5.505 eV for $2H^-$, and 4.750 eV for $H + H^-$),[22,23] and the formation of all nitrogen species. These results indicate that H radicals are the most thermodynamically favored species to generate in H_2–N_2 plasma. This conclusion is consistent with previous studies,[24] which reported that the density of H radicals ($\sim 10^{18}$ m^{-3}) is significantly higher than that of N radicals (10^{14}–10^{17} m^{-3}) and ionic H species (10^{14}–10^{16} m^{-3}) in H_2–N_2 plasma. In addition, the rate coefficient K for H_2 dissociation to H radicals is reported as 8.4×10^{-14} m^3 s^{-1}, which is much higher than the rate coefficient K for H_2 ionization (2.3×10^{-14} m^3 s^{-1}), H_2 dissociative ionization (9.4×10^{-16} m^3 s^{-1}), N_2 dissociation (2.4×10^{-14} m^3 s^{-1}), N_2 ionization (1.4×10^{-14} m^3 s^{-1}) and N_2 dissociative ionization (2.9×10^{-15} m^3 s^{-1}).[24] These reaction kinetics further confirm that H radicals are the most readily generated species in H_2–N_2 plasma. Notably, owing to the strong reducing ability of H radicals, the ground-state N_2 molecules are preferentially reduced by H radicals to form NNH radicals (Fig. 2c) rather than producing N_2^+, N^+, N^- ions or N radicals because of the ultralow energy barrier (0.123 eV) for NNH radical formation, which is significantly lower than the energy barriers for N_2 ionization (15.581 eV),[25] N_2 dissociative ionization (24.449 eV for $N + N^+$, 12.623 eV for $2N^-$, and 11.269 eV for $N + N^-$)[22] and N_2 dissociation into N radicals (9.915 eV). In addition, although the formation energy of H^- ions is higher than that of H radicals, the generated H^- ions can also reduce N_2 to form NNH^- ions with an energy barrier of −0.474 eV. However, considering the density of H radicals is much higher than that of ionic H species in H_2–N_2 plasma,[24,26] the ionic species are not included in our subsequent calculations. Furthermore, we calculated the total NH_3 synthesis reaction pathway under the condition of

 This journal is © The Royal Society of Chemistry 2025

Published on 05 August 2025. Downloaded by Yunnan University on 8/23/2025 4:21:29 PM.

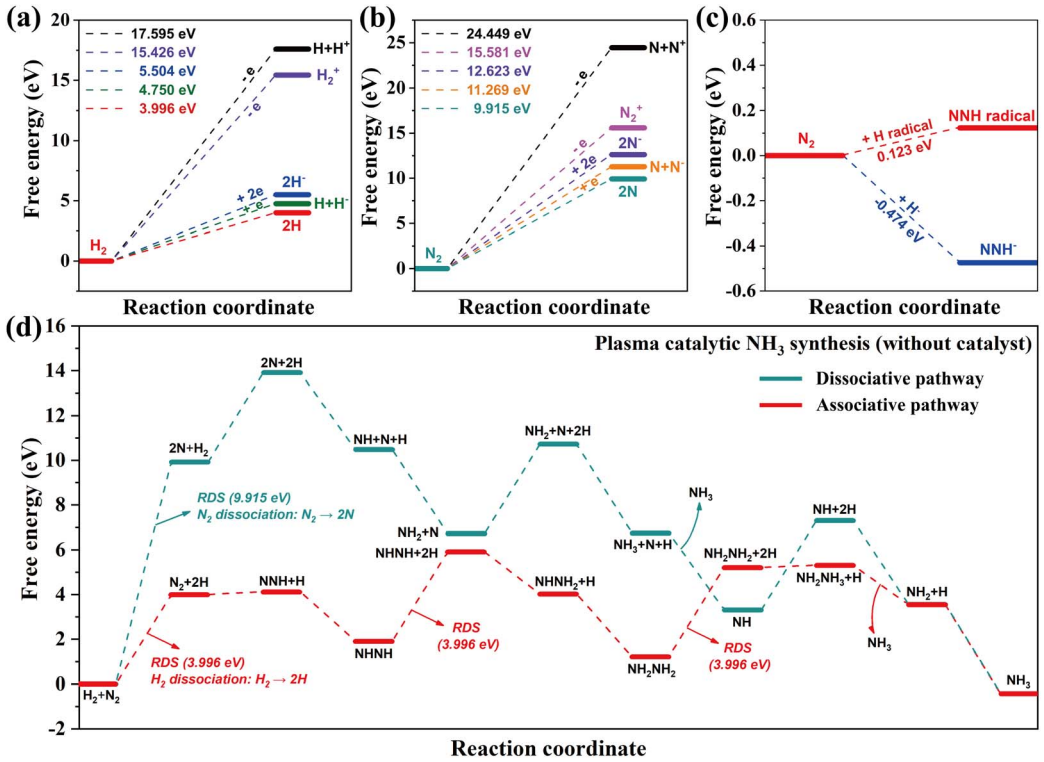

Fig. 2 (a) The free energy diagram for H_2 ionization, H_2 dissociative ionization and bond dissociation of H_2 into H radicals. (b) The free energy diagram for N_2 ionization, N_2 dissociative ionization and bond dissociation of N_2 into N radicals. (c) The free energy profile for the formation of NNH radicals and NNH^- ions. (d) The free-energy profile for the plasma-catalytic NH_3 synthesis (without catalysts) through the dissociative and associative pathways in the gas phase.

sufficient plasma-derived H radicals. As shown in Fig. 2d and S1, the generated H radicals can not only reduce the N_2 molecules but also participate in the subsequent hydrogenation reactions, ensuring that the N≡N bond is cleaved *via* the alternating hydrogenation between two bonding N atoms. This result suggests that the plasma-catalytic NH_3 synthesis preferentially undergoes the associative pathway that no longer needs to directly cleave the N≡N bonds, significantly reducing the required energy input.[27] Based on the above calculations, we deduced that the H radical-mediated associative pathway is the optimal pathway for plasma-catalytic NH_3 synthesis, which indicates that the dissociation of H_2 into H radicals with the energy barrier of 3.996 eV is the rate-determining step of the reaction. Therefore, how to promote the formation of H radicals is the key issue to increase the reaction rate of plasma-catalytic NH_3 synthesis.

Motivated by the DFT results, we selected oxygen-deficient CeO_2 as a catalyst for plasma-catalytic NH_3 synthesis owing to its specificity for accelerating H_2 dissociation, which is crucial for promoting the formation of H radicals.[28–32] As shown in Fig. S2, CeO_2 was first deposited on a CuO support by the hydrothermal method and calcination to obtain CeO_2/CuO, which was then treated with H_2 plasma with an input power of 400 W to produce oxygen vacancies (OVs) on the product surface. The prepared sample was labelled OVs–CeO_2/CuO (Fig. S3). OVs–CeO_2/CuO was further treated with O_2 plasma at 400 W to create the control sample without oxygen vacancies, which was labelled CeO_2/CuO (OV is filled). It is worth noting that the CuO support is only used to facilitate the loading and recovery of the catalyst in the plasma reactor and does not affect the activity of the CeO_2 catalyst, which will be discussed in the following content. The X-ray diffraction (XRD) patterns of all the prepared catalysts matched well with those of cubic CeO_2 (JCPDS 43-1002) and monoclinic CuO (JCPDS 45-0937), demonstrating that the crystal structures of the OVs–CeO_2/CuO and CeO_2/CuO (OV is filled) samples did not change after plasma treatment (Fig. 3a). Electron paramagnetic resonance (EPR) spectroscopy was employed to analyse the oxygen vacancies of the prepared catalysts. As displayed in Fig. 3b, a strong signal at $g = 2.003$ corresponding to the oxygen vacancies was observed for the OVs–CeO_2/CuO catalyst and then disappeared after O_2 plasma treatment. This result indicated that oxygen vacancies can be created and eliminated on CeO_2 through H_2 and O_2 plasma treatment at 400 W, respectively.[33] The creation and elimination of oxygen vacancies on CeO_2 were further identified by O 1s and Ce 3d X-ray photoelectron spectroscopy (XPS). The deconvoluted peaks at 531.4 eV and 885.4 eV clearly indicated the presence of oxygen vacancies[34] and a corresponding increase in the content of Ce^{3+} species in OVs–CeO_2/CuO,[35] respectively (Fig. 3c and d). We also investigated the effect of the input power of H_2 plasma treatment on the generation of oxygen vacancies. The EPR results (Fig. S4) showed that oxygen vacancies were created only when the input power was as high as 400 W.

Published on 05 August 2025. Downloaded by Yunnan University on 8/23/2025 4:21:29 PM.

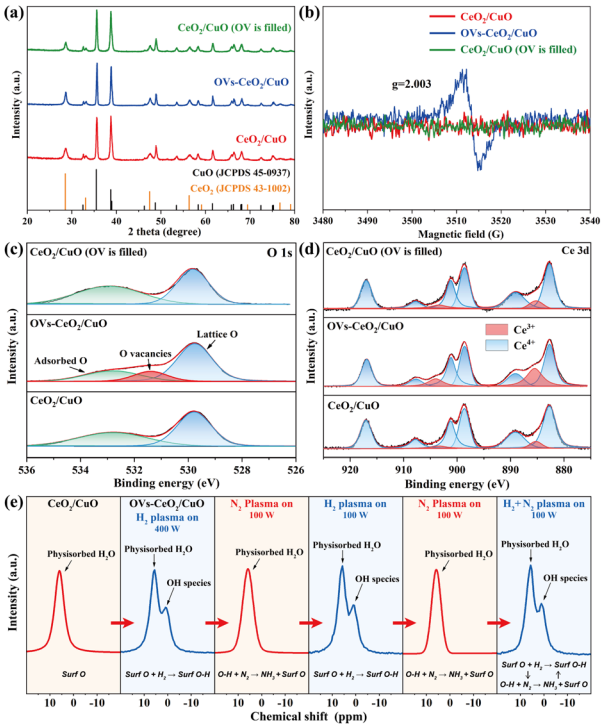

Fig. 3 (a) XRD patterns, (b) EPR results, (c) O 1s XPS spectra, and (d) Ce 3d XPS spectra of CeO_2/CuO, OVs–CeO_2/CuO, and CeO_2/CuO (OV is filled). (e) The ^{1}H NMR spectra of CeO_2/CuO, OVs–CeO_2/CuO, and OVs–CeO_2/CuO treated alternately with N_2, H_2, N_2, and H_2–N_2 plasma at 100 W.

The H_2 dissociation behaviour on the catalyst surface was investigated by solid-state ^{1}H nuclear magnetic resonance (NMR) spectroscopy (Fig. 3e). A characteristic chemical shift corresponding to hydroxyl groups was observed at 0.8 ppm in the spectrum of the fresh OVs–CeO_2/CuO compared with that of CeO_2/CuO, suggesting that the H_2 used in the plasma treatment had already been adsorbed and dissociated by the surface oxygen atoms of OVs–CeO_2/CuO.[36–38] When N_2 and H_2 plasma at 100 W were alternately used to treat OVs–CeO_2/CuO, the hydroxyl groups also alternately disappeared and appeared on the catalyst surface, indicating that chemisorbed hydrogen atoms of the hydroxyl groups can react with N_2 under plasma conditions. Importantly, hydroxyl groups were still detected in the presence of both N_2 and H_2. This result verified that the chemisorbed hydrogen atoms on the catalyst surface were consumed by N_2 and continuously generated through the H_2 dissociation process in H_2–N_2 plasma.

To experimentally investigate the H radical-mediated reaction pathway, the plasma-catalytic NH_3 synthesis experiments were conducted in a dielectric barrier discharge (DBD) reactor (Fig. S5) under optimal conditions. The N_2/H_2 ratio is set at 2/3 to optimize the catalytic performance, while also minimizing excessive H_2 consumption and reducing associated costs (Fig. S6). The maximum reactor power was set at 300 W to ensure that no new oxygen vacancies were created on the catalyst surface during the tests. The NH_3 concentration was measured by Nessler's reagent method (Fig. S7) and further verified with an online mass spectrometer (MS). As displayed in Fig. 4a and b, the OVs–CeO_2/CuO catalyst exhibited an NH_3 yield of 196.2 mg h^{-1} $g_{cat.}^{-1}$ and an energy efficiency of 1.96 g_{NH_3} kWh^{-1} at 100 W, approximately 13 times higher than those of plasma alone. Compared to previously reported catalysts for plasma catalysis, OVs–CeO_2/CuO exhibited the highest NH_3 yield and competitive energy efficiency under similar conditions (Fig. 4c and Table S2).[8,39–46] Furthermore, although the synthesis rate of our catalytic system remains approximately three orders of magnitude lower than that of the high-pressure Haber–Bosch process, it surpasses most of the state-of-the-art thermal catalysts operating under atmospheric pressure conditions (Table S3). After filling the oxygen vacancies with O_2 plasma, the CeO_2/CuO (OV is filled) catalyst shows a significant decrease in NH_3 synthesis performance compared to the OVs–CeO_2/CuO catalyst. The NH_3 yields and energy efficiencies on the CeO_2/CuO (OV is filled) catalyst at all input power points were almost the same as those on the CeO_2/CuO catalyst. Moreover, the OVs–CeO_2/CuO catalysts with different oxygen vacancy concentrations were prepared by controlling the duration of H_2 plasma treatment. As shown in Fig. S8, the catalytic performance of OVs–CeO_2/CuO catalysts increases almost linearly with the concentration of oxygen vacancies, which directly confirmed that the oxygen vacancies enhanced the reaction activity. For further insight into the role of oxygen vacancies in NH_3

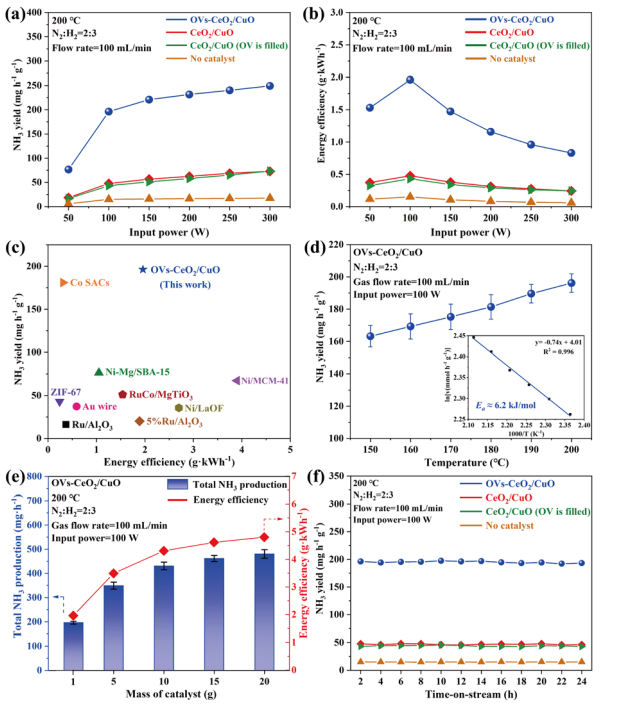

Fig. 4 (a) NH_3 yield, and (b) energy efficiency of different catalysts and plasma alone at various input powers. (c) Performance comparison of OVs–CeO_2/CuO and reported catalysts. (d) The NH_3 yield and Arrhenius plot over the OVs–CeO_2/CuO at temperatures from 423 to 473 K. (e) Total NH_3 production and energy efficiency of different catalyst loading masses of OVs–CeO_2/CuO. (f) Stability tests of plasma-catalytic NH_3 synthesis for 24 continuous hours over different catalysts and plasma alone.

This journal is © The Royal Society of Chemistry 2025

Published on 05 August 2025. Downloaded by Yunnan University on 8/23/2025 4:21:29 PM.

synthesis, the apparent activation energy (E_a) of OVs–CeO_2/CuO was estimated to be 6.2 kJ mol^{-1} by temperature-controlled experiments and an Arrhenius plot (Fig. 4d),[47] which is significantly lower than that of CeO_2/CuO (approximately 40.9 kJ mol^{-1}) (Fig. S9). Furthermore, the discharge properties of plasma (Fig. S10), the materials of the reactor (Fig. S11) and possible environmental pollution (Fig. S12) were investigated to ensure the reliability of all the test results. In addition, almost no ammonia was produced in the absence of plasma discharge, demonstrating the essential role of plasma in our catalytic system (Fig. S13).

We also assessed the industrial application prospects of OVs–CeO_2/CuO by increasing the catalyst loading from 1 g to 20 g. As shown in Fig. 4e, the energy efficiency gradually improved with increasing catalyst loading and reached a superhigh value of 4.8 g_{NH_3} kWh^{-1} (equal to 12.78 MJ $mol_{NH_3}^{-1}$). The value of 12.78 MJ $mol_{NH_3}^{-1}$ was the lowest energy cost among all relevant studies employing the plasma catalysis technique (most values were above 30 MJ $mol_{NH_3}^{-1}$).[48] In addition, the single-pass yield reaches 10.55% when 20 g of the OVs–CeO_2/CuO catalyst is loaded (Fig. S14). These results suggest the preliminary potential of our strategy for industrial scale-up. Stability is another primary concern affecting the applicability of catalysts. As shown in Fig. 4f, all samples exhibited nonsignificant attenuation in NH_3 production during the 24 h continuous test. The OVs–CeO_2/CuO catalyst also showed negligible performance decay and maintained a high NH_3 yield that was almost equal to that observed at the initial stage after 10 times intermittent tests (Fig. S15). Moreover, the XRD, XPS, EPR and SEM results (Fig. S16a–f) confirmed that the crystal structure, elemental valence state, oxygen vacancy concentration, and morphology of OVs–CeO_2/CuO remained essentially unchanged after the test, proving its remarkable stability. Furthermore, the MS measurements (Fig. S17) confirmed that the NH_3 concentration at the outlet remained nearly constant throughout the extended 7-day continuous test, providing strong evidence for the high stability of OVs–CeO_2/CuO. In addition, the thermal stability of the CuO support was also assessed *via* the H_2 temperature programmed reduction (H_2-TPR) method (Fig. S18), confirming the high stability of the CuO support under the applied temperature conditions.[49]

Based on all the aforementioned observations, kinetic experiments and analysis were conducted to unravel the origin of the oxygen vacancies that promoted the dissociation of H_2 molecules. As shown in Fig. 5a and b, the reaction order with respect to P_{N_2} in the plasma + OVs–CeO_2/CuO system was measured to be 0.02, which is very close to 0 and significantly lower than the values of 0.25 for the plasma + CeO_2/CuO system and 0.51 for the only plasma system. Moreover, the reaction order with respect to P_{H_2} in the plasma + OVs–CeO_2/CuO system (0.28) was considerably higher than the 0.16 measured for the plasma + CeO_2/CuO system and the 0.11 measured for the only plasma system. The extremely low reaction order for N_2 and the significantly higher reaction order for H_2 in the plasma + OVs–CeO_2/CuO system confirm that the reaction pathway in the presence of oxygen vacancies is primarily influenced by the H_2 content of the reactants. Thus, we suppose that the plasma-catalytic NH_3 synthesis with the OVs–CeO_2/CuO catalyst was controlled kinetically by the H_2 dissociation process. Subsequently, the H/D kinetic isotopic effects (KIE) were investigated to examine the influence of oxygen vacancies on H_2 dissociation during the plasma-catalytic NH_3 synthesis. As shown in Fig. 5c, the replacement of H_2 with D_2 led to a significant decrease of NH_3 yield on the OVs–CeO_2/CuO catalyst by approximately 19%,

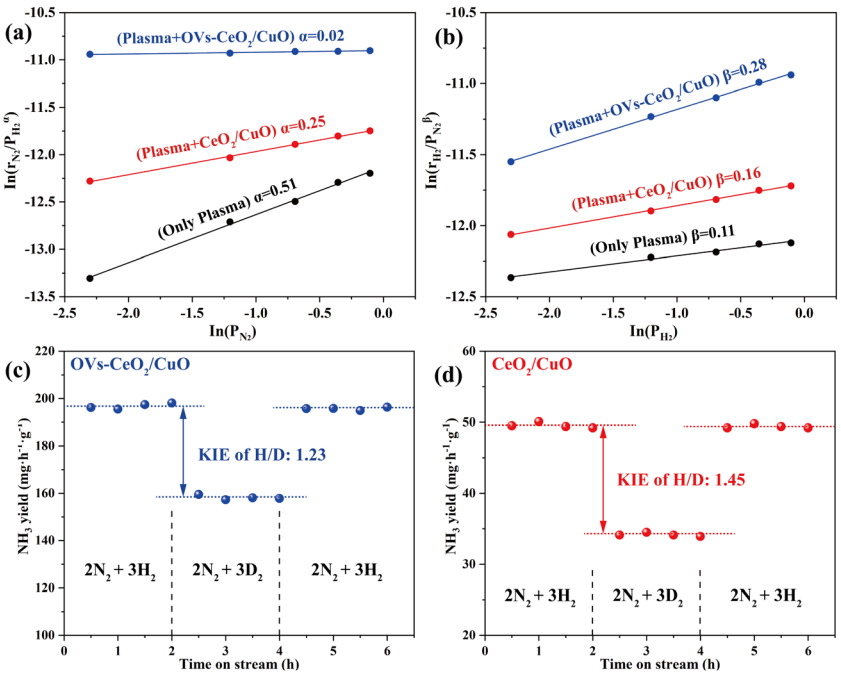

Fig. 5 The dependence of the reaction rate on P_{N_2} (a) and P_{H_2} (b) under plasma-catalytic conditions. The H/D kinetic isotope effects on NH_3 synthesis rates of (c) OVs–CeO_2/CuO and (d) CeO_2/CuO.

Published on 05 August 2025. Downloaded by Yunnan University on 8/23/2025 4:21:29 PM.

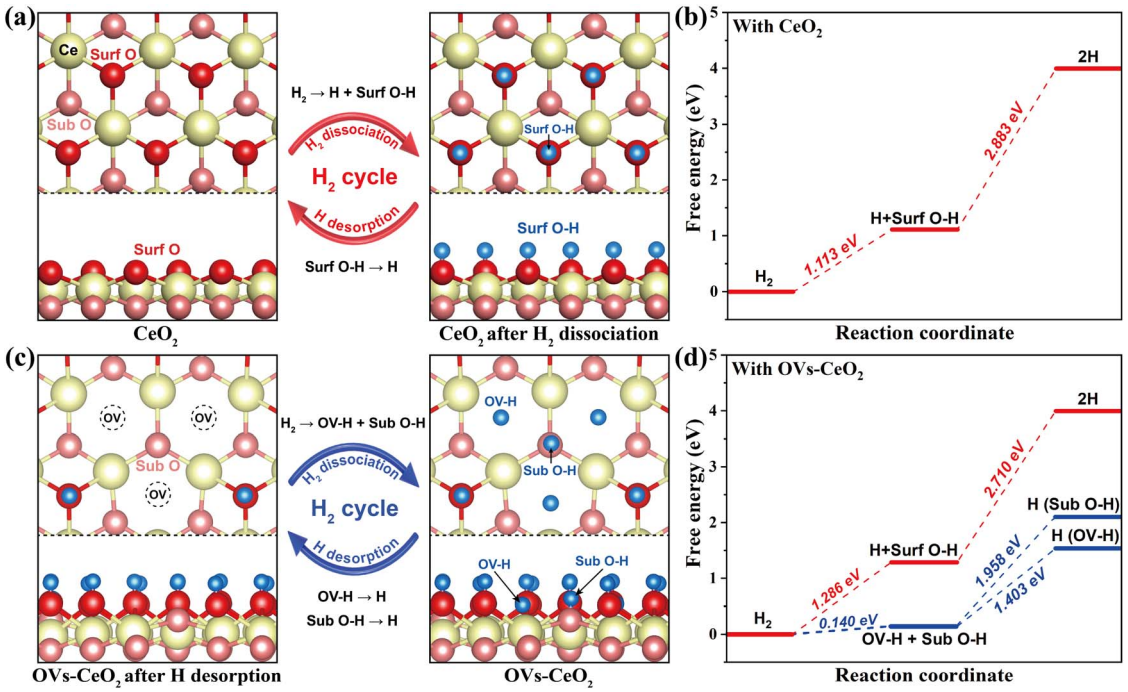

Fig. 6 (a) Surface structures of CeO_2 and that after the H_2 dissociation process. (b) The free-energy diagram for the plasma-catalytic H_2 dissociation with CeO_2. (c) Surface structures of OVs–CeO_2 and that after the H desorption process. (d) The free-energy diagram for the plasma-catalytic H_2 dissociation with OVs–CeO_2.

corresponding to the KIE of 1.23. For comparison, the KIE of CeO_2/CuO was measured to be 1.45 (Fig. 5d), which was significantly larger than that of OVs–CeO_2/CuO, indicating that the oxygen vacancies could accelerate the dissociation rate of H_2, thus promoting the hydrogenation reduction process of N_2 molecules.

Furthermore, we used DFT calculations to reveal how oxygen vacancies affect the dissociation of H_2 and the formation of hydrogen radicals. On the surface of CeO_2, H_2 was first dissociated into surface hydroxyl (O–H) species by surface oxygen atoms (Fig. 6a), and then desorbed to form H radicals (Fig. S19), with an energy barrier of 2.883 eV (Fig. 6b), which is significantly lower than that of 3.996 eV for direct H_2 dissociation without catalysts. After introducing oxygen vacancies (Fig. 6c and S20), the formed oxygen vacancies and the exposed subsurface oxygen atoms dissociated H_2 to form OV-adsorbed hydrogen (OV–H) and subsurface O–H species, which have low H desorption energies of 1.403 eV for OV–H and 1.958 eV for subsurface O–H (Fig. 6d) and thus are more easily desorbed to form hydrogen radicals than the surface O–H species of CeO_2 (2.883 eV). Notably, the H desorption energy of 1.403 eV is significantly lower than that of most transition and precious metals (mostly above 2 eV).[50,51] The lower H desorption energy might be the reason for the superior performance of the OVs–CeO_2/CuO catalyst compared to previously reported metal catalysts (*e.g.* Ni/Al_2O_3,[12] Ru/Al_2O_3,[43] and Co nanoparticles[39]). This result also explains that the reduced E_a of OVs–CeO_2/CuO originates from the enhanced formation of H radicals facilitated by oxygen vacancies. Moreover, the total reaction pathway (Fig. S21 and S22) confirmed that the subsequent N_2 hydrogenation steps were spontaneous and exothermic reactions that could be easily achieved in the gas phase or on the catalyst surface. In summary, DFT calculations demonstrate that the oxygen vacancies significantly reduce the formation energy of H radicals, thereby indirectly promoting the activation and reduction of N_2 and ultimately achieving a high NH_3 synthesis rate (Fig. S23).

To further verify the validity of our catalyst design principle, we used the same method to construct oxygen vacancies in several other metal oxides. As shown in Fig. S24, NiO, Fe_3O_4 and Co_3O_4 exhibited oxygen vacancies and improved NH_3 synthesis performance after H_2 plasma treatment, indicating that this strategy is universal for different metal oxides. To ensure that the CuO support did not affect our test results, we prepared the OVs–CeO_2 powder catalyst from commercial CeO_2 powder. As shown in Fig. S25, the OVs–CeO_2 exhibited performance comparable to that of the OVs–CeO_2/CuO catalyst, indicating that CuO acts solely as a support material to facilitate catalyst loading and recovery. Additionally, the CuO support showed no oxygen vacancies after H_2 plasma treatment, possibly due to its higher vacancy formation energy.[52] DFT calculations (Fig. S26) further suggested that the CuO support exhibited no catalytic activity because hydrogen radicals could not easily form on its surface,[53] which demonstrates that the CuO support does not affect the activity of the CeO_2 catalyst.

Conclusions

In summary, we presented a promising hydrogen radical-mediated N_2 activation pathway for NH_3 synthesis through

 This journal is © The Royal Society of Chemistry 2025

Published on 05 August 2025. Downloaded by Yunnan University on 8/23/2025 4:21:29 PM.

the collective effect of plasma and oxygen-deficient CeO_2/CuO catalysts. This study revealed that oxygen vacancies are crucial for accelerating the dissociation of H_2 and promoting the formation of hydrogen radicals, consequently increasing the intrinsic NH_3 synthesis rate. Benefiting from the above strategies, an impressive NH_3 yield of 196.2 mg h^{-1} $g_{cat.}^{-1}$ was achieved under mild conditions. This study provides novel perspectives into the reaction pathway of plasma-catalytic NH_3 synthesis and proves the significance of the H_2 dissociation step for plasma catalysis. We anticipate that this work will stimulate further exploration of catalyst design using plasma-derived hydrogen radicals.

Author contributions

Siguo Chen, Yanan Chen, and Zidong Wei conceived the project. Shijian Luo performed the catalyst synthesis, structural characterization, performance tests and simulations. Siguo Chen and Shijian Luo analyzed the experimental data. Yongduo Liu performed the DFT calculations. Yang Song, Yuran Yang, Fadong Chen and Linhu Wang assisted in the experimental work. Siguo Chen, Lin Guo, Shijian Luo, and Yongduo Liu discussed the results. Siguo Chen, Lin Guo, and Shijian Luo prepared the manuscript with feedback from other authors. Siguo Chen supervised the project.

Conflicts of interest

There are no conflicts to declare.

Data availability

The data supporting this article have been included as part of the ESI.

Details for the catalysts preparation and experimental process of characterization test; the plasma-catalytic test; the computational study; the kinetic analysis; the study of the universality of catalyst design principles; the comparison of the performance of plasma-catalytic NH_3 synthesis. See DOI: **https://doi.org/10.1039/d5ta04447b**.

Acknowledgements

This research was financially supported by the National Natural Science Foundation of China (Grant No. 22178034 and 21978028, S. C.; Grant No. 22090030 and 52021004, Z. W.), the Chongqing Talent Program (cstc2022ycjh-bgzxm0096, S. C.), and the China Postdoctoral Science Foundation (Grant No. 2023M730399).

Notes and references

1 X. Zhang, Y. Wang, C. Liu, Y. Yu, S. Lu and B. Zhang, *Chem. Eng. J.*, 2021, **403**, 126269.
2 C. Smith, A. K. Hill and L. Torrente-Murciano, *Energy Environ. Sci.*, 2020, **13**, 331–344.
3 R. F. Service, *Science*, 2014, **345**, 610.
4 H. Wu, L. Yang, J. Wen, Y. Xu, Y. Cai, W. Gao, Q. Wang, Y. Guan, S. Feng, H. Cao, T. He, L. Liu, S. Zhang, J. Guo and P. Chen, *Adv. Energy Mater.*, 2023, **13**, 2300722.
5 G. Qing, R. Ghazfar, S. T. Jackowski, F. Habibzadeh, M. M. Ashtiani, C. P. Chen, M. R. Smith and T. W. Hamann, *Chem. Rev.*, 2020, **120**(12), 5437–5516.
6 Y. Xiong, B. Li, Y. Gu, T. Yan, Z. Ni, S. Li, J. L. Zuo, J. Ma and Z. Jin, *Nat. Chem.*, 2023, **15**, 286–293.
7 E. C. Neyts, K. Ostrikov, M. K. Sunkara and A. Bogaerts, *Chem. Rev.*, 2015, **115**, 13408–13446.
8 Y. Wang, W. Yang, S. Xu, S. Zhao, G. Chen, A. Weidenkaff, C. Hardacre, X. Fan, J. Huang and X. Tu, *J. Am. Chem. Soc.*, 2022, **144**, 12020–12031.
9 X. Chen, Y. Duan, J. Wang, X. Yuan, L. Liu, Y. Chen, L. Fu and Y. Wu, *J. Mater. Chem. A*, 2025, **13**, 24824–24830.
10 T.-N. Ye, S.-W. Park, Y. Lu, J. Li, M. Sasase, M. Kitano, T. Tada and H. Hosono, *Nature*, 2020, **583**, 391–395.
11 G. Ertl, *Angew. Chem., Int. Ed.*, 2008, **47**, 3524–3535.
12 Y. Wang, M. Craven, X. Yu, J. Ding, P. Bryant, J. Huang and X. Tu, *ACS Catal.*, 2019, **9**, 10780–10793.
13 C. Ling, X. Niu, Q. Li, A. Du and J. Wang, *J. Am. Chem. Soc.*, 2018, **140**, 14161–14168.
14 Z. Yao, S. Liu, H. Liu, Y. Ruan, S. Hong, T. S. Wu, L. Hao, Y. L. Soo, P. Xiong, M. M. J. Li, A. W. Robertson, Q. Xia, L. X. Ding and Z. Sun, *Adv. Funct. Mater.*, 2023, **33**, 2209843.
15 H. Iriawan, S. Z. Andersen, X. Zhang, B. M. Comer, J. Barrio, P. Chen, A. J. Medford, I. E. L. Stephens, I. Chorkendorff and Y. Shao-Horn, *Nat. Rev. Methods Primers*, 2021, **1**, 56.
16 L. R. Winter, B. Ashford, J. Hong, A. B. Murphy and J. G. Chen, *ACS Catal.*, 2020, **10**, 14763–14774.
17 P. Wang, F. Chang, W. Gao, J. Guo, G. Wu, T. He and P. Chen, *Nat. Chem.*, 2017, **9**, 64–70.
18 K. H. R. Rouwenhorst, Y. Engelmann, K. Van'T Veer, R. S. Postma, A. Bogaerts and L. Lefferts, *Green Chem.*, 2020, **22**, 6258–6287.
19 Z. Qu, R. Zhou, J. Sun, Y. Gao, Z. Li, T. Zhang, R. Zhou, D. Liu, X. Tu and P. Cullen, *ChemSusChem*, 2023, **17**, e202300783.
20 E. Carrasco, M. Jiménez-Redondo, I. Tanarro and V. J. Herrero, *Phys. Chem. Chem. Phys.*, 2011, **13**, 19561–19572.
21 D. Shiner, J. M. Gilligan, B. M. Cook and W. Lichten, *Phys. Rev. A: At., Mol., Opt. Phys.*, 1993, **47**, 4042–4045.
22 J. T. Herron, *J. Phys. Chem. Ref. Data*, 1987, **16**, 1–6.
23 K. R. Lykke, K. K. Murray and W. C. Lineberger, *Phys. Rev. A: At., Mol., Opt. Phys.*, 1991, **43**, 6104–6107.
24 M. Sode, W. Jacob, T. Schwarz-Selinger and H. Kersten, *J. Appl. Phys.*, 2015, **117**, 1–40.
25 T. Trickl, E. F. Cromwell, Y. T. Lee and A. H. Kung, *J. Chem. Phys.*, 1989, **91**, 6006–6012.
26 J. Liu, H. Lu, D. W. Zhang and M. Nolan, *Nanoscale*, 2022, **14**, 4712–4725.
27 A. L. Garden and E. Skúlason, *J. Phys. Chem. C*, 2015, **119**, 26554–26559.
28 Z. Q. Wang, D. R. Chu, H. Zhou, X. P. Wu and X. Q. Gong, *ACS Catal.*, 2022, **12**, 624–632.

Published on 05 August 2025. Downloaded by Yunnan University on 8/23/2025 4:21:29 PM.

29 Z. Zhou, L. Chen, L. Wang, Y. Liu, P. Cheng, H. Peng, J. Cai, Q. Zhou, Y. Wang, N. Yang, B. Wang, X. Q. Gong, F. Yang and Z. Liu, *ACS Catal.*, 2023, **13**, 9588–9596.
30 Z. Li, L. Chen, Z. Wu, A. P. Jia, S. Shi, H. Zhang, J. Wang, Z. Liu, W. P. Shao, F. Yang, X. P. Wu, X. Q. Gong and W. Huang, *ACS Catal.*, 2023, **13**, 5213–5224.
31 Z. Li, K. Werner, K. Qian, R. You, A. Płucienik, A. Jia, L. Wu, L. Zhang, H. Pan, H. Kuhlenbeck, S. Shaikhutdinov, W. Huang and H. J. Freund, *Angew. Chem., Int. Ed.*, 2019, **58**, 14686–14693.
32 C. Riley, S. Zhou, D. Kunwar, A. De La Riva, E. Peterson, R. Payne, L. Gao, S. Lin, H. Guo and A. Datye, *J. Am. Chem. Soc.*, 2018, **140**, 12964–12973.
33 W. Fu, P. Zhuang, M. OliverLam Chee, P. Dong, M. Ye and J. Shen, *ACS Sustain. Chem. Eng.*, 2019, **7**, 9622–9628.
34 R. Jia, Y. Wang, C. Wang, Y. Ling, Y. Yu and B. Zhang, *ACS Catal.*, 2020, **10**, 3533–3540.
35 S. Zhang, Z. Xia, Y. Zou, F. Cao, Y. Liu, Y. Ma and Y. Qu, *J. Am. Chem. Soc.*, 2019, **141**, 11353–11357.
36 J. Wang, Y. Su, J. Xu, C. Ye and F. Deng, *Phys. Chem. Chem. Phys.*, 2006, **8**, 2378–2384.
37 L. Gill, A. Beste, B. Chen, M. Li, A. K. P. Mann, S. H. Overbury and E. W. Hagaman, *J. Phys. Chem. C*, 2017, **121**, 7450–7465.
38 D. M. Lyons, J. P. McGrath and M. A. Morris, *J. Phys. Chem. B*, 2003, **107**, 4607–4617.
39 X. Li, Y. Jiao, Y. Cui, C. Dai, P. Ren, C. Song and X. Ma, *ACS Appl. Mater. Interfaces*, 2021, **13**, 52498–52507.
40 M. Iwamoto, M. Akiyama, K. Aihara and T. Deguchi, *ACS Catal.*, 2017, **7**, 6924–6929.
41 S. Li, Y. Shao, H. Chen and X. Fan, *Ind. Eng. Chem. Res.*, 2022, **61**, 3292–3302.
42 F. Gorky, J. M. Lucero, J. M. Crawford, B. Blake, M. A. Carreon and M. L. Carreon, *ACS Appl. Mater. Interfaces*, 2021, **13**, 21338–21348.
43 S. Li, T. van Raak and F. Gallucci, *J. Phys. D Appl. Phys.*, 2020, **53**, 014008.
44 T. Mizushima, K. Matsumoto, J. I. Sugoh, H. Ohkita and N. Kakuta, *Appl. Catal., A*, 2004, **265**, 53–59.
45 Y. Zhang, S. Li, Z. Yuan, H. Chen and X. Fan, *Ind. Eng. Chem. Res.*, 2022, **61**, 14199–14210.
46 K. Li, S. Chen, H. Wang and F. Wang, *Appl. Catal., A*, 2023, **650**, 118983.
47 J. Li, G. Zhan, J. Yang, F. Quan, C. Mao, Y. Liu, B. Wang, F. Lei, L. Li, A. W. M. Chan, L. Xu, Y. Shi, Y. Du, W. Hao, P. K. Wong, J. Wang, S. X. Dou, L. Zhang and J. C. Yu, *J. Am. Chem. Soc.*, 2020, **142**, 7036–7046.
48 C. Dai, X. Li, M. Zhang, Y. Cui, B. Zhao and X. Ma, *Int. J. Hydrogen Energy*, 2021, **46**, 2213–2224.
49 S. Zeng, T. Chen, K. Liu and H. Su, *Catal. Commun.*, 2014, **45**, 16–20.
50 J. Greeley and M. Mavrikakis, *J. Phys. Chem. B*, 2005, **109**, 3460–3471.
51 P. Nordlander, S. Holloway and J. K. Nørskov, *Surf. Sci.*, 1984, **136**, 59–81.
52 A. Davó-Quiñonero, A. Davó-Quiñonero, A. Davó-Quiñonero, E. Bailón-García, S. López-Rodríguez, J. Juan-Juan, D. Lozano-Castelló, M. García-Melchor, F. C. Herrera, F. C. Herrera, E. Pellegrin, C. Escudero, A. Bueno-López and A. Bueno-López, *ACS Catal.*, 2020, **10**, 6532–6545.
53 Y. Maimaiti, M. Nolan and S. D. Elliott, *Phys. Chem. Chem. Phys.*, 2014, **16**, 3036–3046.

 This journal is © The Royal Society of Chemistry 2025